

X-Ray and Infrared Studies on Superparamagnetic Ni–Zn Ferrite Nanocrystals

D. V. Kurmude · A. B. Shinde · A. A. Pandit ·
C. M. Kale · D. R. Shengule · K. M. Jadhav

Received: 13 November 2014 / Accepted: 18 December 2014 / Published online: 10 January 2015
© Springer Science+Business Media New York 2015

Abstract Series of zinc-substituted nickel ferrite, $\text{Ni}_{1-x}\text{Zn}_x\text{Fe}_2\text{O}_4$ ($x = 0.0, 0.2, 0.4, 0.6, 0.8,$ and 1.0), nanoparticles were synthesized at low temperature by using sol–gel auto-combustion method. Powder X-ray diffraction confirmed the single-spinel structure of the synthesized Ni–Zn ferrite nanocrystals with average crystallite size was found to be 30 nm which is close to that of critical size for exhibiting superparamagnetism which was further verified from Mössbauer spectroscopic studies. The stoichiometric analysis of the ferrite samples carried out by employing energy-dispersive X-ray spectroscopy is found to be as expected. Results of infrared spectroscopic studies carried out on these superparamagnetic ferrite nanocrystals are reported in this paper. The tetrahedral and octahedral absorption band frequencies suggested the spinel structure of the ferrite samples

and its behavior with zinc content x is attributed to the nano-size effect and occupation of zinc cations at the octahedral [B] sites. Further, the force constants are found to be in the reported range of that for ferrites.

Keywords Ni–Zn ferrite nanocrystals · IR absorption bands · Stoichiometry · Superparamagnetism

1 Introduction

Infrared absorption spectroscopy is an important and non-destructive characterizing tool, which provides qualitative information regarding structural details of crystalline materials. The results from IR absorption study can be used to interpret the electrical and magnetic properties of the ferrites. The electric and magnetic properties of these materials are decisively dependent on the precise configuration of the atoms or ions in these structures, and methods of non-destructive analysis are especially suited to such investigations. For example, the vibrational, electronic, and magnetic dipole spectra can give information about the position and valence of the ions in the crystal lattices. The behavior of absorption bands and force constants found to be composition dependent and is attributed to the cation oxygen bond distances in the structure [1].

In particular to ferrite materials, the IR spectroscopic studies are carried out to check the completion of the solid-state reaction, to study the cation distribution, to study the deformation of the spinel structure, cation disordering, and to study the force constants for the tetrahedral and octahedral sites. The ferrites are well known to crystallize in their crystallographic form with space group $Fd_{3m}-O_h^7$. According to group theoretical considerations, four infrared active fundamentals were expected in the vibrational spectra

D. V. Kurmude (✉)
Milind College of Science, Aurangabad,
431004 (M. S.), India
e-mail: dvkurmude@yahoo.com

A. B. Shinde
Aabasaheb Garware College, Pune (M. S.), India

A. A. Pandit
Yashwant College Sillod, Dist. Aurangabad (M. S.), Sillod, India

C. M. Kale
Indraraj Arts Commerce and Science College,
Sillod, Aurangabad, (M. S.), India

D. R. Shengule
Vivekanand Arts, Sardar Dalipsingh Commerce and Science
College, Aurangabad, 431004 (M. S.), India

K. M. Jadhav
Department of Physics Dr. Babasaheb Ambedkar, Marathwada
University, Aurangabad, 431004 (M. S.), India

of normal as well as inverse spinel ferrites. In the frequency range 200–800 cm^{-1} , the spinel ferrites usually show two absorption bands corresponding to the tetrahedral and octahedral sites [2].

Nanosized spinel ferrite particles have attracted considerable interest, and efforts continue to investigate them for their technological applications in the microwave industries, disk recording, refrigeration systems, electrical devices, ferrofluids, etc. The magnetic properties of spinel ferrites can be varied systematically by changing the identity of the divalent metal cations like Co^{2+} , Mn^{2+} , Ni^{2+} , Zn^{2+} , etc. without changing the spinel crystal structure [3].

Among the substituted ferrite materials, nickel–zinc ferrites happen to be the most versatile due to their remarkable magnetic properties such as large permeability at high frequency, remarkably high electrical resistivity, and low power loss [4, 5]. Ni–Zn ferrites possess high thermal stability and high wear and corrosion resistance [6]. Magnetic nanoparticles are attracting researchers not only because of potential use but also for fundamental understanding of their strikingly different properties such as superparamagnetism, quantum magnetic tunneling, and surface spin effects exhibited by them, when its particle size approaches the atomic-scale level [7–11]. Wet, chemically synthesized spinel ferrite nanoparticles exhibit unusual physical properties, as compared to their bulk counterparts [12].

In the present paper, the infrared spectral analysis of superparamagnetic zinc substituted nickel ferrite nanoparticles synthesized by using chemical route of sol–gel auto-combustion is dealt with. Stoichiometry of the ferrite samples is verified using energy-dispersive X-ray spectroscopy, and the obtained results are presented in the paper.

2 Experimental

A series of zinc-substituted nickel ferrite nanoparticles, $\text{Ni}_{1-x}\text{Zn}_x\text{Fe}_2\text{O}_4$ with $0 \leq x \leq 1.0$, by adopting sol–gel auto-combustion method of synthesis is prepared. The nitrates of relevant metals are used as precursors for the synthesis. The obtained ferrite powder is then sintered at 600 °C and used for further studies. Room temperature IR spectra of ferrite powders were recorded using Perkin-Elmer (Model 783) spectrophotometer, in the wave number range of 350 to 1000 cm^{-1} . Stoichiometric study was carried out using Environmental Scanning Electron Microscope having resolution of 3 nm and magnification up to $\times 300,000$ with facility of Secondary and Backscattered Imaging Elemental Analysis (Model SEM: FEI Quanta 200 ESEM). The images were taken at an accelerating voltage of 20 kV. Details of synthesis and Mössbauer spectroscopic studies are already reported [13].

3 Results and Discussion

3.1 X-Ray Diffraction Studies

X-ray diffraction patterns corresponding to $\text{Ni}_{1-x}\text{Zn}_x\text{Fe}_2\text{O}_4$ ferrite system for $x = 0.0, 0.2, 0.4, 0.6, 0.8,$ and 1.0 are recorded at room temperature, and Fig. 1 depicts the typical X-ray diffraction pattern corresponding to $\text{Ni}_{0.4}\text{Zn}_{0.6}\text{Fe}_2\text{O}_4$ composition. The pattern confirms the formation of single-phase cubic spinel structure as the corresponding planes such as (220), (311), (222), (400), (422), (511), and (440) are present in it. Moreover, typical XRD pattern of pure nickel ferrite found to have best match with PDF No. 10-325. The existence of broad peaks in the XRD patterns indicates the nanosize dimensions of the prepared ferrite particles [14]. The lattice constant (a) is calculated by using $a = d(h^2 + k^2 + l^2)^{1/2}$; crystallite size (t) is calculated by using Scherrer's formula; and the cation distribution is estimated by using X-ray intensity calculations as suggested by Buerger [15], and the obtained results are presented in Table 1. Intensity ratios of planes, I_{220}/I_{400} and I_{422}/I_{400} are considered for calculation of cation distribution as they are found to be sensitive [16]. The site radii (r_A) and (r_B) are also calculated from the estimated cation distribution and mentioned in Table 1.

From Table 1, it is clear that the lattice constant (a) increases with zinc substitution as expected. The increasing behavior of lattice constant with Zn^{2+} content is because of replacement of Ni^{2+} ions having comparatively smaller ionic radius (0.69 Å) by Zn^{2+} ions with larger ionic radius (0.74 Å). The variation of the lattice parameter (a) as a function of Zn^{2+} ions concentration (x) in the $\text{Ni}_{1-x}\text{Zn}_x\text{Fe}_2\text{O}_4$ matrix follows Vegard's law [17].

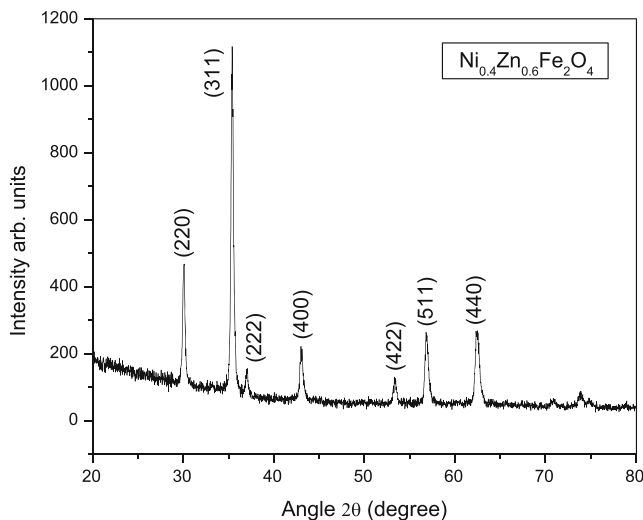


Fig. 1 Typical X-ray diffraction pattern of $\text{Ni}_{0.4}\text{Zn}_{0.6}\text{Fe}_2\text{O}_4$ recorded at room temperature

Table 1 Lattice constant (a), crystallite size (t), cation distribution, and site radii (r_A and r_B) of the $\text{Ni}_{1-x}\text{Zn}_x\text{Fe}_2\text{O}_4$ ferrite nanoparticles obtained from X-ray diffraction studies

x	a (Å)	t (nm)	A site	B site	r_A (Å)	r_B (Å)
0.0	8.328	41	(1Fe)	[1Ni ₁ Fe]	0.645	0.668
0.2	8.356	32	(0.0Ni _{0.1} Zn _{0.9} Fe)	[0.8Ni _{0.1} Zn _{1.10} Fe]	0.655	0.668
0.4	8.377	27	(0.26Ni _{0.0} Zn _{0.74} Fe)	[0.34Ni _{0.4} Zn _{1.26} Fe]	0.657	0.672
0.6	8.405	30	(0.2Ni _{0.0} Zn _{0.8} Fe)	[0.2Ni _{0.6} Zn _{1.2} Fe]	0.654	0.678
0.8	8.428	30	(0.08Ni _{0.0} Zn _{0.92} Fe)	[0.12Ni _{0.8} Zn _{1.08} Fe]	0.649	0.686
1.0	8.431	34	(0.0Ni _{0.02} Zn _{0.98} Fe)	[0.0Ni _{0.98} Zn _{1.02} Fe]	0.647	0.692

Particle size of pure nickel ferrite is obtained to be 41 nm. Upon substitution of zinc, it was found to be reduced to average value of 30 nm. The presence of zinc obstructs the crystal growth in spinel ferrites as the formation of zinc ferrite is more exothermic as compared to formation of nickel ferrite. Thus, it is expected that if one introduces zinc in the system, more heat will be liberated, decreasing the molecular concentration at the crystal surface and hence obstructing the grain growth [18] and reducing the particle size. Further, smaller particle size of the samples doped with zinc ions is due to lower bond energy of $\text{Zn}^{2+}-\text{O}^{2-}$ as compared to that of $\text{Ni}^{2+}-\text{O}^{2-}$ [19]. The reduction in particle size of a ferrite material produces interesting changes in ionic distributions of the spinel structure which in turn can give rise to enhanced magnetic properties. To calculate the X-ray diffraction intensities (I_{hkl}) instead of considering all the planes of the spinel, typical planes namely (220), (400), (422), and (440) are considered, as these planes are known to be cation sensitive planes [20].

Also from Table 1, it is seen that the pure nickel ferrite shows inverse spinel structure as expected with all the Ni^{2+} ions situated at the octahedral [B] sites along with half of the Fe^{3+} ions and remaining half of Fe^{3+} ions at the tetrahedral (A) sites. Strikingly, it is also seen from Table 1 although Zn^{2+} ions have strong preference to the tetrahedral (A) sites in bulk zinc ferrite; the Zn^{2+} ions have been found to be situated at the octahedral [B] sites with large degree of inversion. This may be attributed to the method of synthesis and nano size of the prepared ferrite samples [21–23].

3.2 Energy Dispersive X-Ray Spectroscopic Studies

The chemical composition of the sol–gel synthesized $\text{Ni}_{1-x}\text{Zn}_x\text{Fe}_2\text{O}_4$ ferrite samples with $x = 0.0, 0.2, 0.4, 0.6, 0.8,$ and 1.0 was also analyzed by energy-dispersive X-ray spectroscopy (EDS). The EDS patterns of all the compositions of Ni–Zn ferrite system over different areas of the

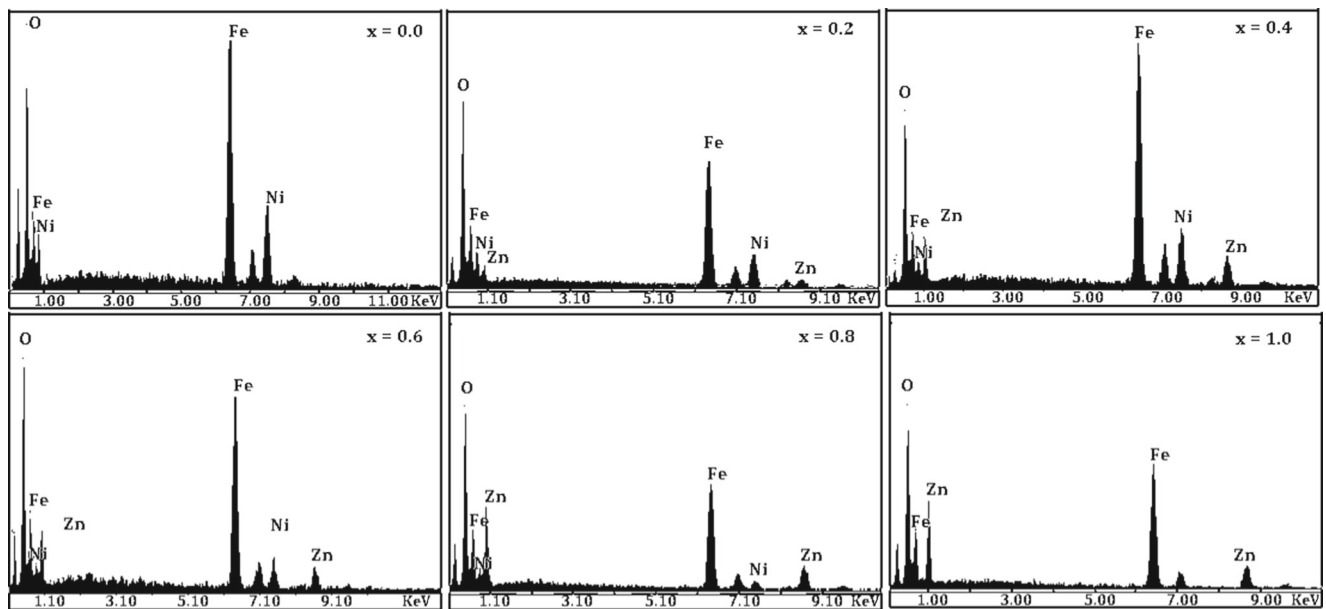


Fig. 2 EDS spectra of $\text{Ni}_{1-x}\text{Zn}_x\text{Fe}_2\text{O}_4$ ferrite samples with $x = 0.0, 0.2, 0.4, 0.6, 0.8,$ and 1.0

Table 2 Chemical composition (wt%) of the $\text{Ni}_{1-x}\text{Zn}_x\text{Fe}_2\text{O}_4$ ferrite nanoparticles obtained from energy-dispersive X-ray spectroscopy (EDS) and its expected values

x	Chemical composition (wt%)							
	Ni		Zn		Fe		O	
	Obs.	Exp.	Obs.	Exp.	Obs.	Exp.	Obs.	Exp.
0.0	0.2742	0.2504	0.0000	0.0000	0.5068	0.4766	0.2190	0.2730
0.2	0.1962	0.1992	0.0694	0.0555	0.4703	0.4738	0.2641	0.2715
0.4	0.1377	0.1485	0.1113	0.1103	0.4731	0.4712	0.2779	0.2700
0.6	0.0996	0.0985	0.1726	0.1646	0.4671	0.4685	0.2607	0.2684
0.8	0.0485	0.0490	0.2263	0.2182	0.4214	0.4659	0.3038	0.2669
1.0	0.0000	0.0000	0.2403	0.2712	0.4580	0.4633	0.3017	0.2655

specimen under investigation are recorded at 20 kV, and typical patterns are shown in Fig. 2.

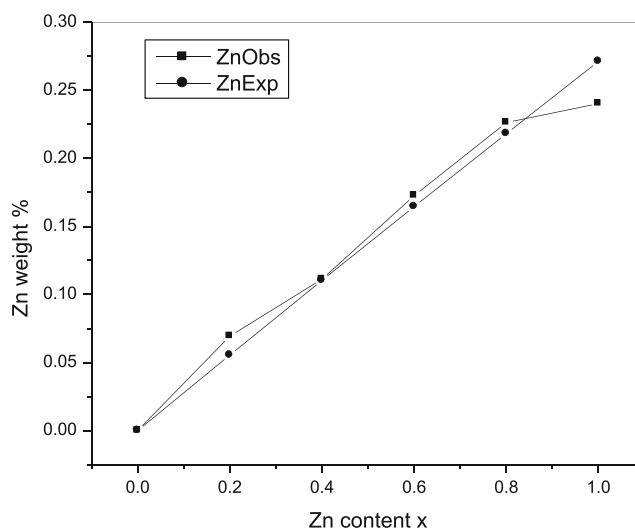
It is well known that the energy-dispersive X-ray spectroscopy conveniently gives the effective atomic concentration of different constituents on top surface layers of the solid investigated. It is seen that no element other than nickel, zinc, ferric, and oxygen is present in the prepared samples, and obviously, the synthesized sample is chemically pure and possesses desired stoichiometry. The elemental weight percentages of the constituent elements in the Ni–Zn ferrite nanoparticles were also obtained from energy-dispersive X-ray spectroscopic studies and compared with their stoichiometric values. These values are presented in Table 2. It is seen that the calculated weight percentage of Ni, Zn, and Fe values matches well with the amount of Ni, Zn, and Fe used in the respective precursors.

A comparison of initial substitution levels of Zn^{2+} and the average levels in synthesized individual particles measured via EDS are given in Fig. 3. It is seen that these values matches well with each other. Further, the surface concentrations of nickel, zinc, ferric, and oxygen species are found to be closer to each other in almost all the cases. Such closeness of the values indicates the homogeneous distribution of nickel, zinc, ferric, and oxygen species in the synthesized samples. Thus, the combustion route easily controls the stoichiometry and crystallite size which further have strong influence on structural, morphology, magnetic, and electric properties of ferrites [24]. Thus, it can be concluded that all the samples prepared by sol–gel synthesis technique were formed with the desired stoichiometry. The purity of the samples is maintained within the experimental errors.

3.3 Infrared Spectroscopic Studies

IR absorption spectra of the ferrite samples under investigation are shown in Fig. 4. The magnetic properties of

the ferrite materials are decisively dependent on the precise configuration of the atoms or ions in the structure. According to R. D. Waldron, infrared spectroscopy provides useful information about the structure of molecule rapidly and also without tedious calculations. And for this purpose, the intensities of bands associated with the tetrahedral (A) and octahedral [B] sites; ν_1 and ν_2 , respectively, are considered [25]. The observed absorption (minimum % transmission) band frequencies and other relevant parameters corresponding different vibration bands of $\text{Ni}_{1-x}\text{Zn}_x\text{Fe}_2\text{O}_4$ ferrite samples with $x = 0.0, 0.2, 0.4, 0.6, 0.8,$ and 1.0 are given in Table 3. In general, these vibrational frequencies depend on cation mass, cation–oxygen distance, and the bonding force [26]. The difference in the $\text{Fe}^{3+}\text{–O}^{2-}$ distance for the tetrahedral and octahedral complexes is reflected in the band

**Fig. 3** Comparison of initial substitution levels of Zn^{2+} and the average levels in synthesized individual particles measured via EDS of $\text{Ni}_{1-x}\text{Zn}_x\text{Fe}_2\text{O}_4$ ferrite samples with $x = 0.0, 0.2, 0.4, 0.6, 0.8,$ and 1.0

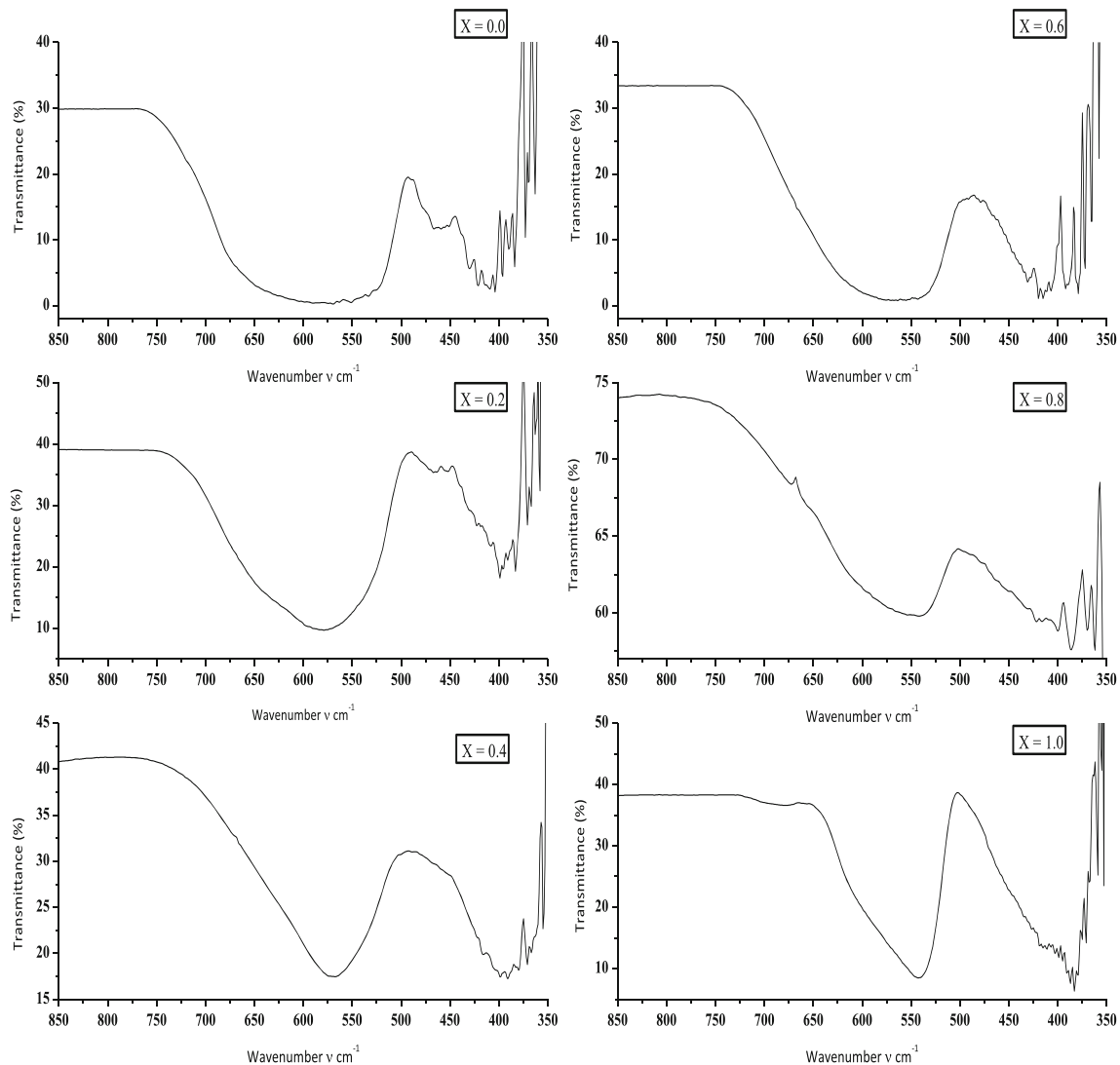


Fig. 4 Room temperature IR spectra of $\text{Ni}_{1-x}\text{Zn}_x\text{Fe}_2\text{O}_4$ ferrite samples with $x = 0.0, 0.2, 0.4, 0.6, 0.8,$ and 1.0

positions of ν_1 and ν_2 . The values of ν_1 are higher than those of ν_2 , indicating that the normal mode of vibration of the tetrahedral complexes is higher than that of corresponding the octahedral site. This is as expected because of the shorter bond length of the tetrahedral (A) site ($R_A = 1.89 \text{ \AA}$) than that of the octahedral [B] site ($R_B = 1.99 \text{ \AA}$) [27–29].

The values of the absorption band frequencies (ν_1, ν_2) of pure nickel (587 cm^{-1} and 396 cm^{-1}) and pure zinc (540 cm^{-1} and 393 cm^{-1}) ferrites are in agreement with those observed by R. D. Waldron. Similarly, Zahi assigned a band at $\sim 570 \text{ cm}^{-1}$ to the tetrahedral bond stretching and the band at $\sim 418 \text{ cm}^{-1}$ to the vibration in the octahedral site of the composition $\text{Ni}_{0.5}\text{Zn}_{0.5}\text{Fe}_2\text{O}_4$ [30]. The slight deviations in the values may be due to different synthesis method and variations in the synthesis parameters.

Also, it is to be noted that the values for pure zinc ferrite are less than those for pure nickel ferrite nanoparticles.

Thus, it is expected for a mixed system of Ni–Zn ferrite that the absorption band position should shift towards lower wavelength side on substitution of zinc for nickel. From Table 3, it is clear that the tetrahedral absorption band position ν_1 has been shifted from 570 cm^{-1} to 543 cm^{-1} and the octahedral absorption band position ν_2 is shifted from 404 cm^{-1} to 388 cm^{-1} .

It is known that increase in the site radius (r_B) (Table 3) hinders the fundamental frequency, and therefore the center frequency ν_2 should shift towards lower frequency side [31]. It is also seen that initially up to zinc content $x = 0.2$ ν_1 increases; ν_2 decreases, and then with increase in zinc concentration, the frequency ν_1 decreases and the ν_2 increases similar to the reports [32–34]. In the present study, the zinc ions were found to occupy the octahedral [B] sites from cation distribution studies. Cation distribution study has also revealed that the pure nickel is an inverse spinel

Table 3 IR absorption bands (ν) and calculated force constants (k) of the $\text{Ni}_{1-x}\text{Zn}_x\text{Fe}_2\text{O}_4$ ferrite nanoparticles

x	ν_1 (cm^{-1})	ν_2 (cm^{-1})	k_t (dyne/cm)	k_o (dyne/cm)
0.0	570	404	1.38	0.99
0.2	579	399	1.45	0.97
0.4	567	371	1.39	0.85
0.6	564	379	1.37	0.90
0.8	544	386	1.26	0.95
1.0	543	388	1.26	0.97

ferrite as usual, but the substitution of zinc in place of nickel pushes the nickel ions to the tetrahedral (A) sites. Therefore, the observed shifting of ν_2 from zinc content $x = 0.2$ towards higher wave number side may be due to presence of zinc ions at the octahedral sites with its larger ionic radius of 0.74 \AA (nickel 0.69 \AA) than that of Fe^{3+} (0.645 \AA) ions, thereby pushing Fe^{3+} ions towards oxygen ion resulting in reduced $\text{Fe}^{3+}-\text{O}^{2-}$ bond length, and as there is an inverse relation between wave number and bond length [35, 36].

From Table 3, it is also seen that the values of stretching vibrations observed at both sites show a slight change with increasing Zn content, and this behavior is in good agreement with the variation in site radii (Table 1) [37]. The variation of these two band positions as a function of Zn content (x) is shown Fig. 5. It is clear that the absorption band frequencies ν_1 and ν_2 related to the tetrahedral (A) and octahedral [B] sites vary in opposite manner with the Zn content (x) in the $\text{Ni}_{1-x}\text{Zn}_x\text{Fe}_2\text{O}_4$ ferrite composition. Similar results are reported by Kumar Mohit et al. [38].

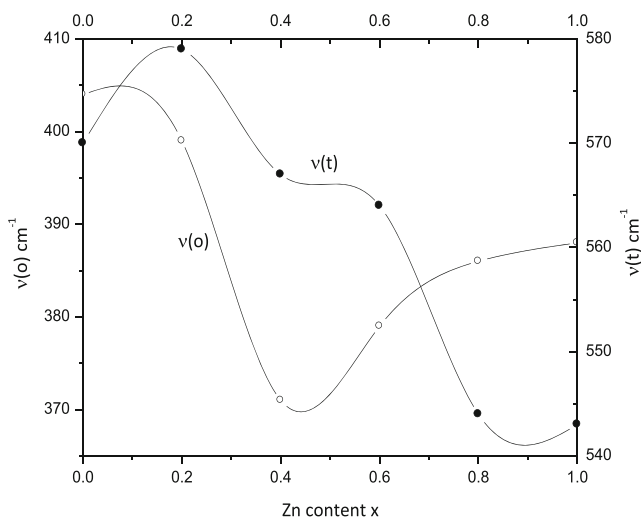


Fig. 5 Variation of IR absorption band frequencies (ν_1 and ν_2) as a function of Zn content x in $\text{Ni}_{1-x}\text{Zn}_x\text{Fe}_2\text{O}_4$ ferrite system with $x = 0.0, 0.2, 0.4, 0.6, 0.8,$ and 1.0

Mössbauer studies of similar compositions [39, 40] revealed that neither all Ni^{2+} ions should go to the [B] sites nor should all Zn^{2+} ions exist in the (A) sites but a mixed cationic distribution may exist depending on the Ni^{2+} to Zn^{2+} ratios and few other parameters. Mössbauer studies on the present Ni–Zn ferrite system has also been carried out and previously and the results have shown mixed cationic distribution. For ready reference, a typical Mössbauer spectrum of $\text{Ni}_{0.6}\text{Zn}_{0.4}\text{Fe}_2\text{O}_4$ ferrite powder obtained for the present Ni–Zn ferrite system indicating clearly superparamagnetic doublet along with the regular sextet is reproduced in Fig. 6, and details of the Mössbauer studies are reported earlier [13]. Further, the presence of isolated superparamagnetic clusters at the [B] sites screened by the diamagnetic Zn^{2+} ions has been observed in Ni–Zn ferrites by Mössbauer studies [41]. These may be the reasons for the observed change in band positions.

The force constant corresponding to the tetrahedral (A) site (K_t) and octahedral [B] site (K_o) were estimated by employing the method suggested by R. D. Waldron.

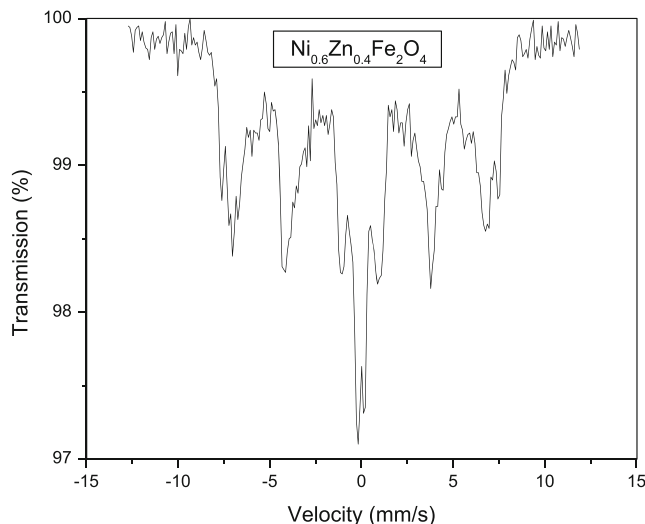


Fig. 6 Typical Mössbauer spectrum of $\text{Ni}_{0.6}\text{Zn}_{0.4}\text{Fe}_2\text{O}_4$ ferrite powder obtained at room temperature

The obtained values of the force constants are listed in Table 3. The values of the force constants are in good agreement with values of the tetrahedral and octahedral absorption frequencies. Force constants are proportional to the strengths of interatomic bonding at (A) and [B] sites. Furthermore, the calculated values of (K_t) are greater than those of (K_o). However, the values of the bond length of (A) site (R_A) are smaller than those of [B] site (R_B) as mentioned earlier. This is due to the inverse proportionality between the bond length and the force constants [42].

Far IR absorption spectra of the Ni–Zn-mixed ferrite nanoparticles shown in Fig. 4 also exhibit few weaker bands below ν_2 in some compositions. These weaker bands may be probably due to is divalent metal ion (Fe^{2+})–oxygen (O^{2-}) complexes in the octahedral sites. It is worth noting that hopping electrons between Fe^{2+} ions and Fe^{3+} ions simultaneously existing in the octahedral sites are responsible for transportation mechanisms in ferrites [43]. Some of these are also can be due to lattice vibrations [27, 44]. The broadening of bands has been reported earlier by many workers [45]. Such broadening is attributed to statistical distribution of Fe^{3+} ions in the tetrahedral (A) and octahedral [B] sites based on stoichiometric composition. Broadening of peaks gives idea about structure of the ferrite; whether it is normal or inverse.

4 Conclusions

The infrared spectroscopic studies carried out on the superparamagnetic nickel zinc ferrite nanoparticles reflects the structural changes as seen from the behavior of the tetrahedral and octahedral absorption band frequencies in regard with the levels of zinc substitution and occupancy of zinc ions at the octahedral sites. Further, the force constants also vary accordingly. The results of energy-dispersive X-ray spectroscopic studies confirmed the desired stoichiometry of the ferrite samples.

Acknowledgments One of the authors, D. V. Kurmude, is thankful to the head of the Department of Physics, Shivaji University Kolhapur for providing the IR facility.

References

- Ladgaonkar, B.P., Kolekar, C.B., Vaingankar, A.S.: Bull. Mater.Sci. **25**, 4 (2002)
- Shaikh, A.M., Jadhav, S.A., Watawe, S.C., Chougule, B.K.: Mater. Lett. **44** (2000)
- Koseoglu, Y., Bay, M., Tan, M., Baykal, A., Sozeri, H., Topkaya, R., Akdogan, N.: J. Nanopart. Res. (2010). doi:10.1007/s11051-010-9982-6
- Sharma, S., Verma, K., Chaubey, U., Singh, V., Mehta, B.R.: Sci. Eng. B **167**, 3 (2010)
- Virden, A.E., Grady, K.O.: J. Magn. Magn. Mater., 290 (2005)
- Costa, A.C.F.M., Silva, V.J., Cornejo, D.R., Morelli, M.R., Kiminami, R.H.G.A.: J. Magn. Magn. Mater. **320**, 14 (2008)
- Kodama, R.H., Berkowitz, A.E.: Phys. Rev. B **59**, 9 (1999)
- Fatemi, D.J., Harris, V.G., Chen, M.X., Malik, S.K., Yelon, W.B., Long, G.J., Mohan, A.: J. Appl. Phys. **85**, 8 (1999)
- Chen, J.P., Sorensen, C.M., Klabunde, K.J., Hadjipanayis, G.C., Devlin, E.: Kostikas, A.: Phys. Rev. B **54**, 13 (1996)
- Hamdeh, H.H., Ho, J.C., Oliver, S.A., Willey, R.J., Oliveri, G., Busca, G.: J. Appl. Phys. **81**, 4 (1997)
- Oliver, S.A., Harris, V.G., Hamdeh, H.H., Ho, J.C.: Appl. Phys. Lett. **76** (2000)
- Modi, K.B., Rangolia, M.K., Chhantbar, M.C., Joshi, H.H.: J. Mater. Sci. **41**, 22 (2006)
- Kurmude, D.V., Kale, C.M., Aghav, P.S., Shengule, D.R., Jadhav, K.M.: J. Supercond. Nov. Magn. **27**, 8 (2014)
- Hankare, P.P., Patil, R.P., Sankpal, U.B., Jadhav, S.D., Mulla, I.S., Jadhav, K.M., Chougule, B.K.: J. Magn. Mag. Mater. **321**(19) (2009)
- Buerger, M.G.: Crystal structure analysis. Wiley, New York (1960)
- Pandit, A.A., More, S.S., Dorik, R.G., Jadhav, K.M.: Bull. Mater. Sci **26**(5) (2003)
- Kumar, P., Mishra, P., Sahu, S.K.: Inter. J. Scien. Eng. Res. **2**(8) (2011)
- Chandan Upadhyay, H.C., Verma, J.: Appl. Phys. **95**(10) (2004)
- Ibrahim Sharifi, H., Shokrollahi, J.: Magn. Mag. Mater., 324 (2012)
- Ohinishi, H., Teranishi, T.: J. Phys. Soc. Jpn. **16** (1961)
- Hamdeh, H.H., Ho, J.C., Oliver, R.J., Willey, J., Kramer, Y.Y., Chen, S.H., Lin, Y.D., Yao, M., Daturi, G.: IEEE Busca Trans. Magnet. **31**(6) (1995)
- Battle, J., Clark, T., Evans, B.J.: J. Phys. IV France **7** (1997)
- Navrotsky, A., Kleppa, O.J., Inorg, J.: Nucl. Chem. **30**, 479 (1968)
- Deraz, N.M., Alarifi, A.: vol. 7 (2012)
- Waldron, R.D.: Phys. Rev. **99**, 6 (1955)
- Patil, S.A., Mahajan, V.C., Ghatage, A.K., Lotke, S.D.: Mater. Chem. Phys. **57**, 1 (1998)
- Mazen, S.A., Metawe, F., Mansour, S.F.: J. Phys. D **30**, 12 (1997)
- Evans, B.J., Hafner, S.: J. Phys. Chem. Solids **29**, 9 (1968)
- Mazen, S.A., Mansour, S.F., Dhahri, E., Zaki, H.M., Elmosalami, T.A.: J. Alloy. Comp. **470**, 1-2 (2009)
- Zahi, S.: J. Electrom. Anal. Appl. **2** (2010)
- Bhatu, S.S., Lakhani, V.K., Tanna, A.R., Vasoya, H., Buch, J.U., Sharma, P.U., Trivedi, U.N., Joshi, H.H., Modi, K.B.: Ind. J. Pure. Appl. Phys. **45** (2007)
- Saafan, S.A., Meaz, T.M., El-Ghazzawy, E.H., El Nimr, M.K., Ayad, M.M., Bakr, M.: J. Magn. Magn. Mater. **322** (2010)
- Priyadharsini, P., Pradeep, A., Rao, P.S., Chandrasekaran, G.: Mater. Chem. Phys. **116**, 1 (2009)
- Kaiser, M.: J. Alloy. Comp. **468**, 1–2 (2009)
- Sujatha, Ch., Reddy, K.V., Babu, K.S., Reddy, A.R.C., Rao, K.H.: Physica. B **407** (2012)
- Singh, N., Agarwal, A., Sanghi, S., Khasa, S.: J. Magn. Magn. Mater. **324** (2012)

37. Gabal, M.A., El-Shishtway, R.M., Al-Angari, Y.M.: *J. Magn. Magn. Mater.* **324**, 14 (2012)
38. Mohit, K., Rout, S.K., Parida, S., Singh, G.P., Sharma, S.K., Pradhan, S.K., Kim, I.W.: *Phys. B Condens. Matt.* **407** (2012)
39. Arshed, M., Siddique, M., Anwar-ul-Islam, M., Butt, N.M., Abbas, T., Ahmed, M.: *Solid St. Comm.* **93**, 7 (1995)
40. Attia, S.M.: *Egyp. J. Solid* **29**, 2 (2006)
41. Josyulu, O.S., Sobhanadri, J.: *Phys. Stat. Sol. A* **65**, 2 (1981)
42. Watawe, S.C., Sutar, B.D., Sarwade, B.D., Chougule, B.K.: *Internal. J. Inorg. Mater.* **3**, 7 (2001)
43. Reddy, P.V., Reddy, V.D.: *J. Magn. Magn. Mater.* **136**, 3 (1994)
44. Puri, R.K., Varshney, U.: *J. Phys. Chem. Solid* **44**, 7 (1983)
45. Modi, K.B., Gajera, J.D., Pandya, M.P., Vora, H.G., Joshi, H.H.: *Pramana J. Phys* **62**, 5 (2004)